Fatigue Crack Paths in the VHCF-regime of 100Cr6

P. Grad[1] and E. Kerscher[1]

[1] University of Kaiserslautern, Working Group of Materials Testing,
Gottlieb-Daimler-Str., D-67663 Kaiserslautern, Germany. grad@mv.uni-kl.de (P. Grad)

ABSTRACT. *Cyclically loaded machine parts made of high strength-steel mostly fail at high lifetimes from subsurface inclusions. This phenomenon was observed notably in fatigue tests at low stress amplitudes, which cause failure in the very high cycle fatigue (VHCF) regime. In contrast, at high stress amplitudes the crack initiation and failure starts from the surface. It can be shown that, depending on stress level, different crack growth mechanisms play an essential role for the failure from subsurface inclusions. To analyse the crack growth initiated from inclusions, specimens of the bearing steel 100Cr6 in martensitic condition were tested under tension-compression at different loads till failure. The fracture surfaces were analysed by a scanning electron microscope (SEM) with focus on the crack origin, to apply fracture mechanics theory. In combination to this the microstructure below the crack surface was analysed in detail by a focused ion beam (FIB) preparation of the area around the inclusion and a transmission electron microscopy (TEM) observation. Finally the change of failure mode is explained by different crack growth mechanisms, which depend on the respective stress intensity factors and a general threshold value for the initiation of long cracks.*

INTRODUCTION

Recent years have produced an increased number of studies of the fatigue behaviour of materials at very high numbers of cycles ($> 10^7$) and associated low stress amplitudes below the classical fatigue limit. The reason for the intensive interest in this topic is given by the requirement of higher lifetimes of cyclic loaded machine parts e.g. high pressure pumps for gasoline direct injection systems [1]. Especially in high-strength steels under cyclic loading no fatigue limit could be found. Additionally, it has been reported by many researchers that the fatigue behaviour could not be described by a classic S-N curve. Instead, a two-part S-N curve has been noted resulting from a change in the crack initiation site from surface to subsurface defects. At high stress amplitudes and low numbers of cycles a fatigue crack initiation from surface is found. In contrast, at low stress amplitudes and high numbers of cycles an internal fatigue crack initiation takes place. Here, an initiation from non-metallic inclusions is characteristic for high-strength steels [2-5].

On fracture surfaces induced by subsurface inclusions it is possible to detect different types of crack propagation mechanisms. An internal crack always forms a so called

fisheye with the character of a long crack propagation. Within the fisheye a fine granular area in the vicinity of the non-metallic inclusion appears at low stress levels or small inclusion sizes, where the crack propagation mechanism is unknown. It is necessary to find the mechanism for formation of this area in order to understand the change in failure mode and the very high cycle fatigue.

The aim of this work is to clarify the mechanisms of change of failure mode in high-strength steels in the VHCF-regime. For this purpose tension-compression fatigue tests were carried out. The fracture surfaces were analysed by SEM, FIB and TEM. The change in failure mode is discussed by fracture mechanics adapted for crack initiation starting from inclusions.

MATERIAL AND EXPERIMENTAL SETUP

Testing Material and Specimen

Fatigue tests were performed with high-purity bearing steel 100Cr6 (material number 1.3505, AISI 52100, JIS SUJ2). The chemical composition in we.-% is 1.47 Cr, 0.95 C, 0.29 Si, 0.25 Mn, 0.04 Cu, 0.017 Mo, 0.003 P and 0.002 S. The fatigue specimens were quenched in oil after 20 min at 840°C and tempered for 120 min at 180°C. Figure 1 shows the generated martensitic microstructure. This heat treatment resulted in a content of 16,3 ± 1,4 vol.-% retained austenite and a Vickers hardness of 780 HV.

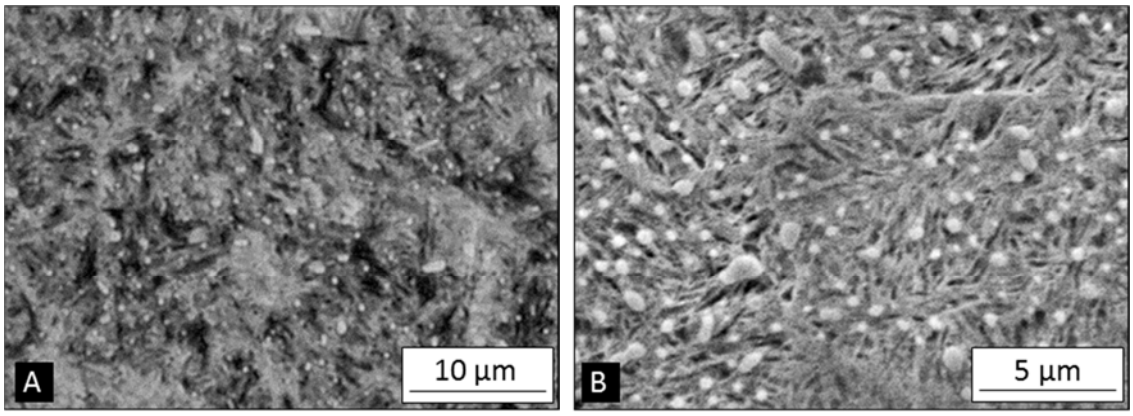

Figure 1. Martensitic microstructure by optical microscope (A) and by SEM (B)

Hour-glass shaped specimens for fatigue tests were machined with oversize, heat treated, and then grinded. Compressive residual stresses of about 400 MPa were measured on the grounded specimen surface, which declined to 0 MPa at 10 µm below the surface. For this reason a smooth polishing was applied to reduce the residual stresses in surface. The elastic stress concentration factor of the specimen is 1.027. The highly stressed volume of the specimen has a diameter of 4.0 mm and a length of 5.0 mm.

Testing Methods

Fatigue tests were performed at room temperature in ordinary room atmosphere using an ultrasonic fatigue testing machine, which was operated at 20 kHz. In this study tension-compression fatigue tests with sinusoidal wave were carried out under an applied stress ratio, R, of -1. To prevent an abnormal heating of the specimen as a result of the high testing frequency, the specimens were tested by ultrasonic pulse-pause-cycles. Additionally, the specimens were cooled by compressed air and the specimen temperature was monitored by an infrared temperature sensor. The maximum allowed temperature difference in reference to room temperature was 15 K.

RESULTS AND DISCUSSION

S-N curve

Figure 2 shows the S-N curve resulting from the fatigue experiments. The analysis of the position of crack initiating inclusions resulted in a two-part S-N curve. The data points marked with a rhombus show the specimens with crack initiation starting from non-metallic inclusions on the surface. Specimens with subsurface initiated failure are marked by a square.

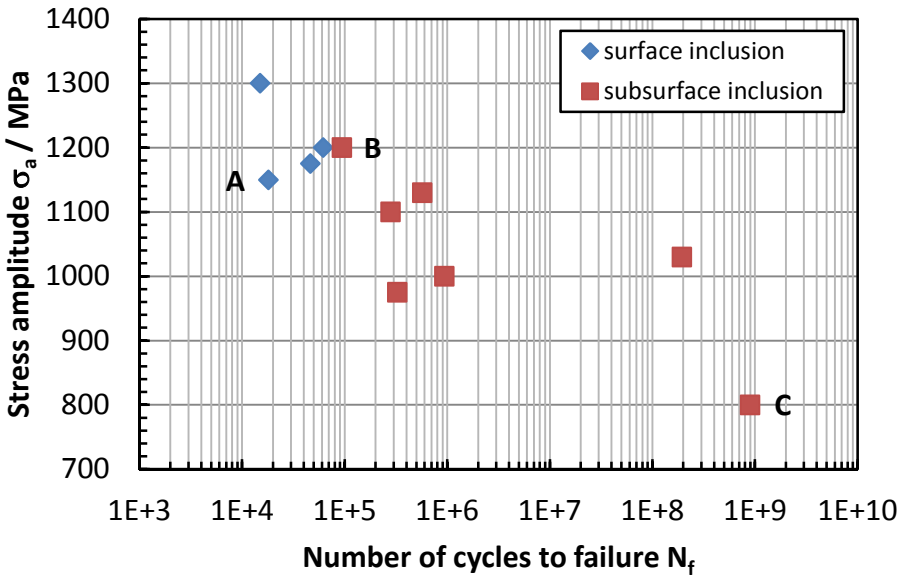

Figure 2. S-N curve of 100Cr6 in martensitic condition

Thus it appears that there is a change in fatigue crack initiation site from surface inclusions at high stress amplitudes and low numbers of cycles to subsurface inclusions at low stress amplitudes and high numbers of cycles. Furthermore the fatigue experiments show a large scatter in lifetime, which is typical for high-purity high strength steels [6]. Figure 3 shows SEM-pictures of the fracture surfaces of the specimens marked with A, B, C in Fig. 2. The different crack paths are indicated by

arrows describing the direction of crack propagation. The three observations are exemplarily for the fracture modes, which were observed in the fatigue experiments. Whereas a crack initiates directly from surface inclusions and grows from there into the material's volume (Fig. 3A), a crack from subsurface inclusions first grows in a so called fisheye ringlike into the surrounding material until the fisheye comes up to the surface of the fatigue specimen. Then such a crack grows further from the surface into the material (Fig. 3B) [7]. The second-mentioned fracture mode occurs when the critical stress intensity factor for unstable crack growth is not reached before the crack forming the fisheye tangents the surface. Otherwise a residual fracture takes place, even when the fisheye has not yet spread to the surface. Characteristic for the fracture surface within the fisheye is a smooth crack path, especially in comparison to the crack path from surface into the materials depth, which is the same at fracture surfaces of specimens with a direct initiation at the surface inclusions. The longer crack path from subsurface inclusions leads to higher number of cycles as it is confirmed by fatigue test results [7]. A specific characteristic of specimens which failed at high numbers of cycles from subsurface inclusions is a rough area around the inclusion within the fisheye (Fig. 3C). The mechanisms forming this area are still unclear, but there are indications that this area is responsible for the failure at high numbers of cycles. In literature different names like ODA (optical dark area) [8], FGA (fine granular area) [2] or GBF (granular bright facet) [9] exist for this area, depending on the postulated mechanism or the observation method. We call this area FGA according to [2].

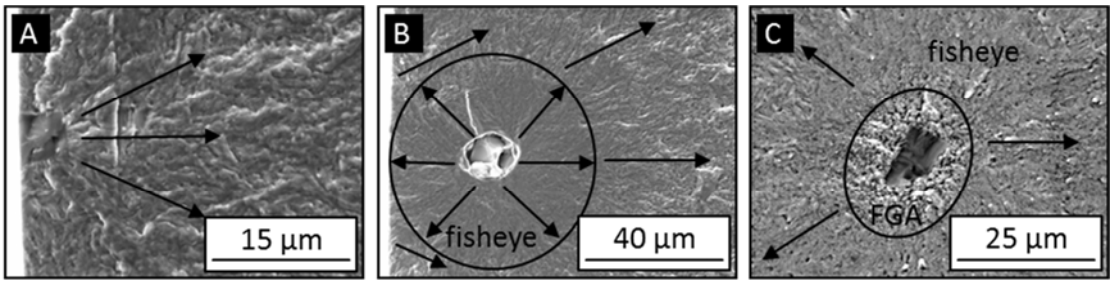

Figure 3. SEM observation of fracture surfaces with different crack initiation and propagation modes

Fracture mechanics adapted for inclusions

To explain the occurence of the different crack paths and the change in failure mode of subsurface inclusions, fracture mechanics is applied to calculate stress intensity factors for the different crack surface morphologies of the fracture surfaces. On the basis of Murakami's equations [10] the inclusions and FGAs are valued by the size and the applied stress amplitude. The relation between stress intensity factors and numbers of cycles to failure are plotted in Fig. 4. Like in Fig. 2 the different crack initiation sites are marked by different symbols. The dashed line marks the threshold value , K_{th}, for a crack initiation from surface inclusions given by [9]. Fig. 4 shows a decrease of the inclusion stress intensity factors with increasing numbers of cycles. There is still a

failure initiated from subsurface inclusions even if the stress intensity factor is below the threshold value of 4 MPa $m^{1/2}$ for surface inclusions. In view of fracture mechanics these inclusions should not be critical for a crack initiation and no failure should occur. In contrast, specimens with stress intensity factors at subsurface inclusions greater than 4 MPa $m^{1/2}$ show crack initiation and failure is possible. Comparing the fracture surfaces of the two different groups of subsurface inclusions it is conspicuous that only the inclusions with stress intensity factors below the threshold value are surrounded by a FGA. Therefore Fig. 4 also shows the stress intensity factors calculated with the area of the FGAs and the stress amplitude. These stress intensity factors take a value in the range of K_{th} independent of the number of cycles.

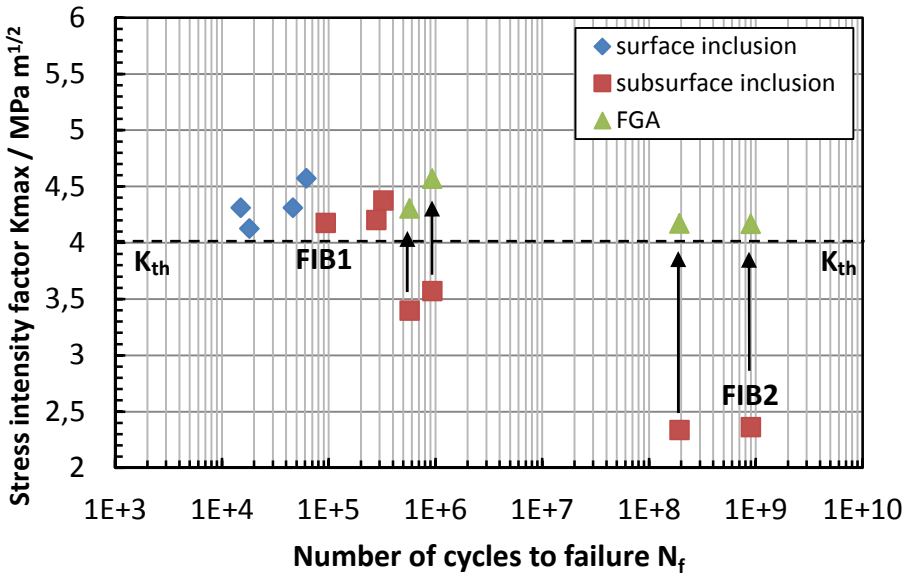

Figure 4. Relationship between stress intensity factor and number of cycles to failure

So it can be concluded, that the mechanism of FGA-forming appears only when the stress intensity factor of crack initiating subsurface inclusions is less than 4 MPa $m^{1/2}$. In addition, the formation of the FGA and the associated mechanisms are responsible for the crack initiation at or around inclusions with stress intensity factors less than 4 MPa $m^{1/2}$ and for the fatigue fracture in the regime of very high cycles, where normally no fracture should occur. Once the area of the FGA around the inclusion has reached the size which results in a stress intensity factor equal to the threshold value, the mechanism changes and the crack propagates in forming the fisheye, which has the same morphology like the area around inclusions with stress intensity factors greater than the threshold value. Until now it is not clear which mechanism leads to the formation of the FGA. The next chapter should clarify this question.

Crack Paths from subsurface inclusions

For a better understanding of the VHCF-behavior and the crack initiation at subsurface inclusions the microstructure in the inclusion surrounding area is analysed by a FIB-

preparation. At first a fracture surface showing an inclusion without FGA is prepared. Figure 5 shows the cross section cut through the inclusion and the inclusion surrounding area of the fracture surface of the specimen marked in Fig. 4 by ‘FIB 1’.

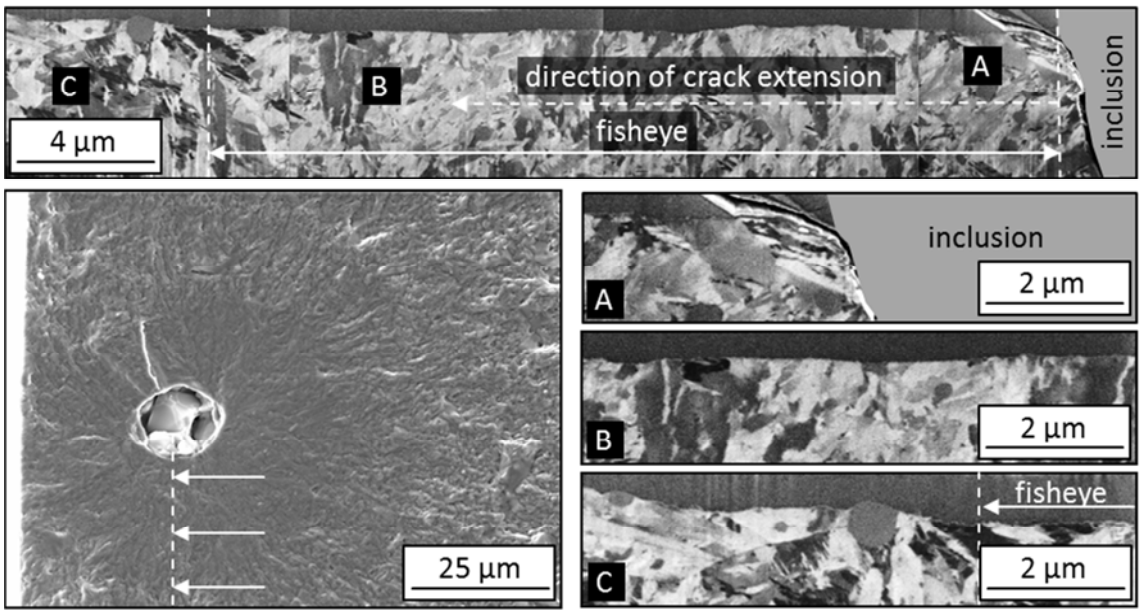

Figure 5. Cross section preparation through an inclusion surrounded by a fisheye

The dashed line in the SEM-picture of the fracture surface shows the position of the cross section. The viewing direction on the cross section is marked by the arrows. It is obvious from the detailed view in Fig. 5A that the crack started directly at the inclusion with a vertical orientation to the main normal stress. Thus within the fisheye there is a straight line visible for the crack propagation path which starts from the inclusion and is independent of the microstructure (Figs 5A and 5B). The transition of fisheye crack growth mode to crack growth from surface marked by the dashed line in Fig. 5C can be observed by a change in surface roughness. Outside of the fisheye the topography changes in a rougher crack propagation mode. This transition is explained by the absence of ambient air during fisheye crack growth [11].

Figure 6 also shows a cross section of the specimen marked in Fig. 4 by ‘FIB 2’. In contrast to the specimen which is analysed in Fig. 5, the inclusion in this fracture surface is surrounded by a FGA within the fisheye. The position and viewing direction of the cut is also shown analogously to Fig. 5. By the different surface roughnesses, which are clearly visible in the cross section cut, the FGA (Fig. 6A) and the fisheye (Fig. 6B) can be easily separated. Within the FGA a very rough fracture surface is observed in comparison to the fisheye. The direction of crack extension is only known in the fisheye, because within the FGA the crack propagation mechanismen is unclear. Additionally, it seems that the crack propagation depends on microstructure and is not ideally vertically orientated to the main normal stress. It follows that the crack growth mechanism which occurs in the fisheye is different from the mechanism that takes place

in the FGA. Whereas a long crack propagation occurs in the fisheye, the FGA shows a type of short crack growth, which needs to be analysed in more detail.

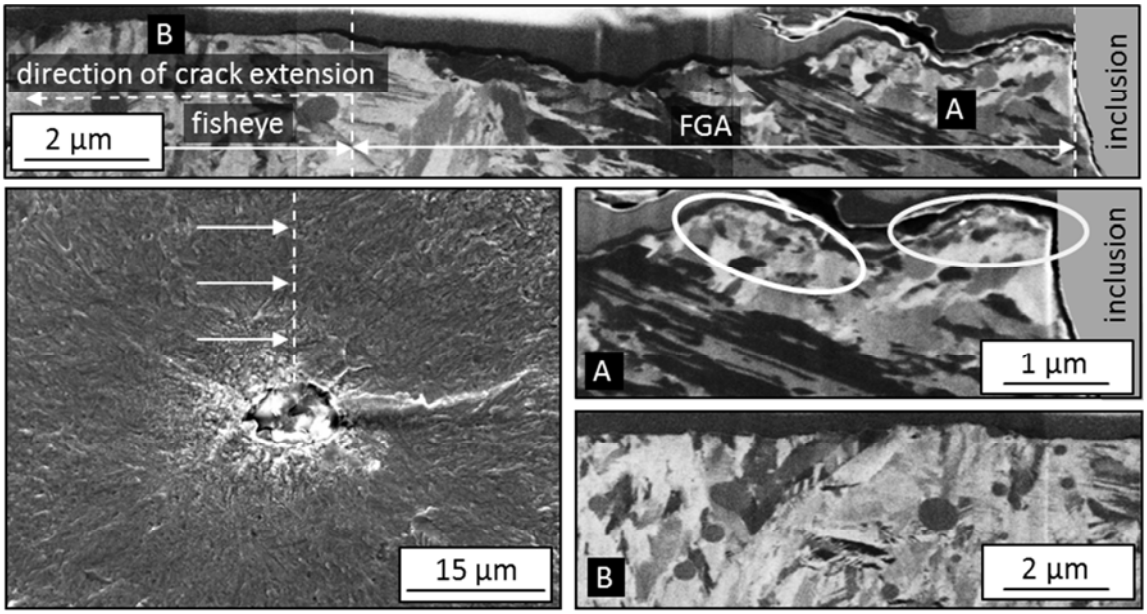

Figure 6. Cross section through inclusion, FGA and fisheye

Another characteristic of the FGA is a fine granular part in the microstructure just below the crack path, as seen at higher magnification in Fig. 6A. Investigations by TEM (Fig. 7) showed that the grain size within those fine granular parts is far below 100 nm. In comparison, the average grain size in the original material is about 1-2 µm. In conclusion the FGA is not merely a fine granular looking area at the fracture surface, but the FGA consists of a fine granular microstructure at and below the crack path.

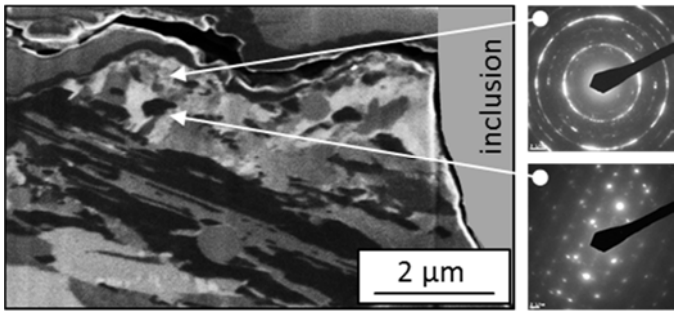

Figure 7. Selected area diffraction pattern by TEM

As mentioned above, different mechanisms for forming the FGA have been postulated in the literature. Our investigations seem to support the postulated mechanism of Sakai et. al. [2]. They explain the formation of this area by three steps: at first a

polygonization around the inclusion takes place during cyclic loading; then follows a nucleation and coalescence of micro-debondings; and finally all micro-debondings form the FGA. But some questions still remain: Why should the polygonizated area get exactly so large that the threshold value is reached? Is it really only a polygonization within the FGA, while our diffraction patterns clearly show rings, which are typical of a configuration of several grains with large angle grain boundaries within the spot size? So the remaining question is whether the FGA could be created by a recrystallization of the original microstructure during the fatigue loadings.

CONCLUSION

The investigations showed the key function of the FGA-formation for the crack initiation at inclusions in the VHCF-regime. The formation of this area occurs exclusively at subsurface inclusions with stress intensity factors less than the threshold value. Looking at FGA forming mechanisms as postulated in the literature, own investigations can be interpreted in support of Sakai's mechanism, although there are still some unclear points which would require further investigation.

ACKNOWLEDGMENTS

The authors would like to thank the Deutsche Forschungsgemeinschaft (DFG) for financially supporting this project.

REFERENCES

1. Bacher-Hoechst, M., Issler, S. (2011). In: *VHCF5 Proceedings*, pp. 45-50, Berger, C., Christ, H.-J. (Ed.), DVM, Berlin.
2. Sakai, T., Sato, Y., Oguma, N. (2002) *Fatigue Fract. Eng. Mater. Struct.* **25**, 765-773.
3. Kerscher, E., Lang, K.-H., Löhe, D. (2008) *Mater. Sci. Eng., A* **483-484**, 415-417.
4. Shiozawa, K., Lu, L., Ishihara, S. (2001) *Fatigue Fract. Eng. Mater. Struct.* **24**, 781-790.
5. Tanaka, K., Akiniwa, Y. (2002) *Fatigue Fract. Eng. Mater. Struct.* **25**, 775-784.
6. Kerscher, E., Lang, K.-H., Löhe, D. (2011) *Procedia Eng.* **10,** 1985-1990.
7. Grad, P., Reuscher, B., Brodyanski, A., Kopnarski, M., Kerscher, E. (2011) In: *Fortschritte in der Metallographie*, pp. 177-182, Wanner, A., Rettenmayr, M. (Ed.), DGM, Frankfurt.
8. Murakami, Y., Nomoto, T., Ueda, T. (1999) *Fatigue Fract. Eng. Mater. Struct.* **22**, 581-590.
9. Shiozawa, K., Morii, Y., Nishino, S., Lu, L. (2006) *Int. J. Fatigue* **28**, 1521-1532.
10. Murakami, Y., Kodama, S., Konuma, S. (1989) *Int. J. Fatigue* **11**, 291-298.
11. Nakamura, T., Oguma, H., Shinohara, Y. (2010) *Procedia Eng.* **2**, 2121-2129.